nature physics

SUPPLEMENTARY INFORMATION

https://doi.org/10.1038/s41567-019-0682-6

In the format provided by the authors and unedited.

Cooling and self-oscillation in a nanotube electromechanical resonator

C. Urgell[1,4], W. Yang[1,4*], S. L. De Bonis[1], C. Samanta[1], M. J. Esplandiu[2], Q. Dong[3], Y. Jin[3] and A. Bachtold[1*]

[1]ICFO - Institut De Ciencies Fotoniques, The Barcelona Institute of Science and Technology, Castelldefels, Spain. [2]Catalan Institute of Nanoscience and Nanotechnology, CSIC and BIST, Campus UAB, Bellaterra, Spain. [3]Centre de Nanosciences et de Nanotechnologies, CNRS, Université Paris-Sud, Université Paris-Saclay, Palaiseau, France. [4]These authors contributed equally: C. Urgell, W. Yang. *e-mail: wei.yang@icfo.eu; adrian.bachtold@icfo.eu

Supplementary Information
Cooling and Self-Oscillation in a Nanotube Electro-Mechanical Resonator

C. Urgell, W. Yang, S. L. de Bonis, C. Samanta,
M. J. Esplandiu, Q. Dong, Y. Jin, and A. Bachtold

I. CALIBRATION OF THE DISPLACEMENT

In order to quantify the displacement using Eqs. 3,4 in methods, we estimate the capacitance C_{g} from the separation $\Delta V_{\mathrm{g}} = 23.1$ mV between two conductance peaks in the Coulomb blockade regime at large positive V_{g} values (Fig. S1). We obtain $C_{\mathrm{g}} = e/\Delta V_{\mathrm{g}} = 6.94 \times 10^{-18}$ F. We get $C_{\mathrm{g}}' = 7 \times 10^{-12}$F/m from the measurement of the variance of the displacement as a function of temperature using $m = 2.7$ ag.

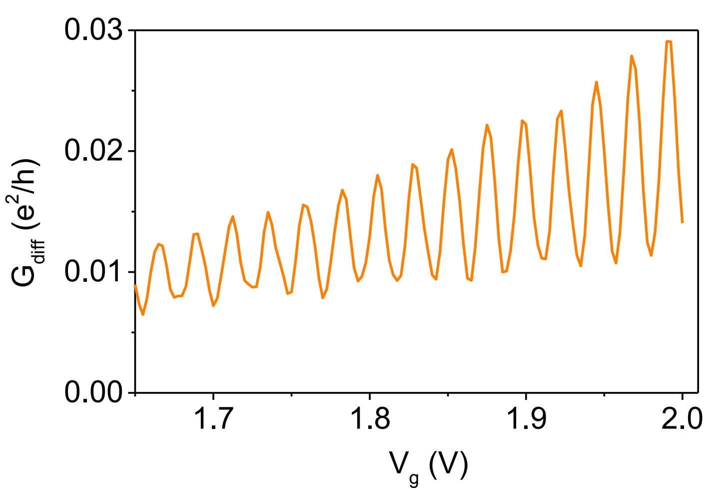

FIG. 1. **Coulomb blockade measurements.** Differential conductance G_{diff} as a function of gate voltage at 10 K and zero source-drain bias.

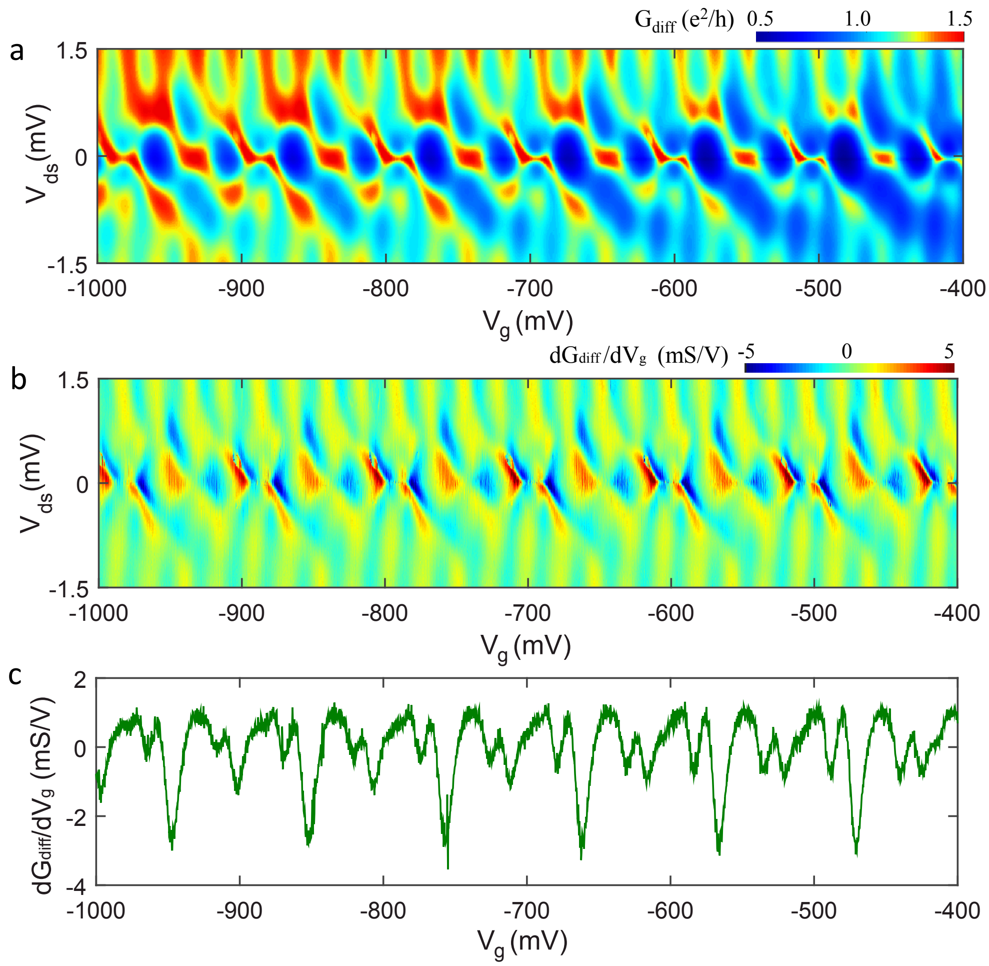

FIG. 2. **Electron transport measurements. (a,b)** Differential conductance and transconductance as a function of V_{sd} and V_{g} measured at the base temperature of the fridge. **(c)** Transconductance as a function of V_{g} measured at $V_{\mathrm{sd}} = 0.7$ mV.

II. RELATION BETWEEN ELECTRON TRANSPORT AND VIBRATION COOLING

Figures S2a,b show that the measurements of G_{diff} and $\frac{dG_{\mathrm{diff}}}{dV_{\mathrm{g}}}$ as functions of V_{g} and V_{sd} are remarkably regular over a large range of gate voltage. This reflects the high quality of the nanotube. The shell filling with Kondo ridges at zero source-drain bias is observed over the full range of V_{g}. The instability in the conductance discussed in Figs. 1b and 2d of the main text appears periodically in gate voltage over the full V_{g} range as well.

Figures S2b,c show that regions with strongly negative $\frac{dG_{\mathrm{diff}}}{dV_{\mathrm{g}}}$ emerge periodically in V_{g} at finite source-drain voltage. This occurs for V_{sd} in the range between 0.4 mV and 1.1 mV.

We observe efficient cooling in these strongly negative $\frac{dG_{\mathrm{diff}}}{dV_{\mathrm{g}}}$ regions, as demonstrated by the measured spectra of thermal vibrations in Figs. S3a-c.

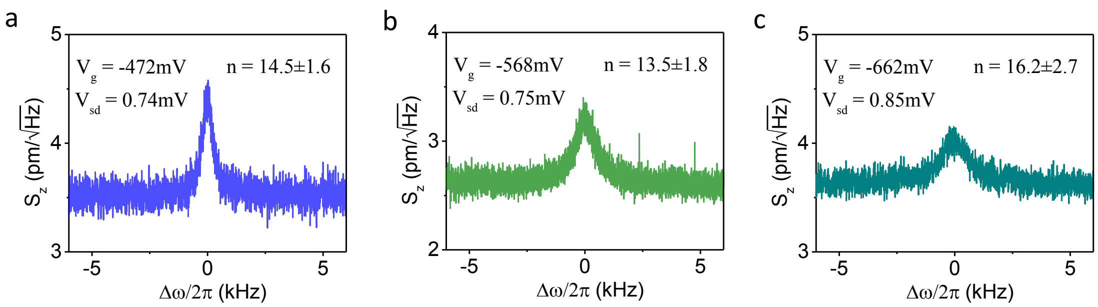

FIG. 3. **Cooling at different V_{g} values. (a-c)** Displacement power spectral density of thermal vibrations showing low occupation number in regions where $\frac{dG_{\mathrm{diff}}}{dV_{\mathrm{g}}}$ is strongly negative.

III. SELF-OSCILLATION

The vibrations of the nanotube in the instability region switch back and forth between thermal motion and self-oscillation, as it can be seen in the time traces of one of the two quadratures (X) and of the amplitude (R) in Fig. S4. In these traces, the amplitude of thermal vibrations is low, whereas the amplitude in self-oscillation is high. These switches between thermal motion and self-oscillation occur randomly in time.

Pure self-oscillation can also be observed without any switches to thermal vibrations. See for instance Fig. S5. This often happens at high V_{sd} values.

IV. SHOT NOISE MEASUREMENT

Here we describe how we measure the shot noise of the nanotube device. The spectral density of the current noise S_{II} is transformed into spectral density of voltage noise S_{VV} through the total impedance $Z_{\mathrm{tot}} = (R_{\mathrm{diff}}^{-1} + Z_{\mathrm{RLC}}^{-1})^{-1}$, where R_{diff} is the nanotube differential resistance and Z_{RLC} is the effective impedance of the RLC circuit. The voltage fluctuations, which are amplified by the high-electron-mobility-transistor amplifier (HEMT), are measured at the frequency $\omega_{\mathrm{RLC}} = 2\pi \cdot 1.27$ MHz over $\sim$ 80kHz bandwidth. Our noise measurement contains the background contribution $S_{\mathrm{II}}^{\mathrm{bg}}$ related to the Johnson-Nyquist noise of

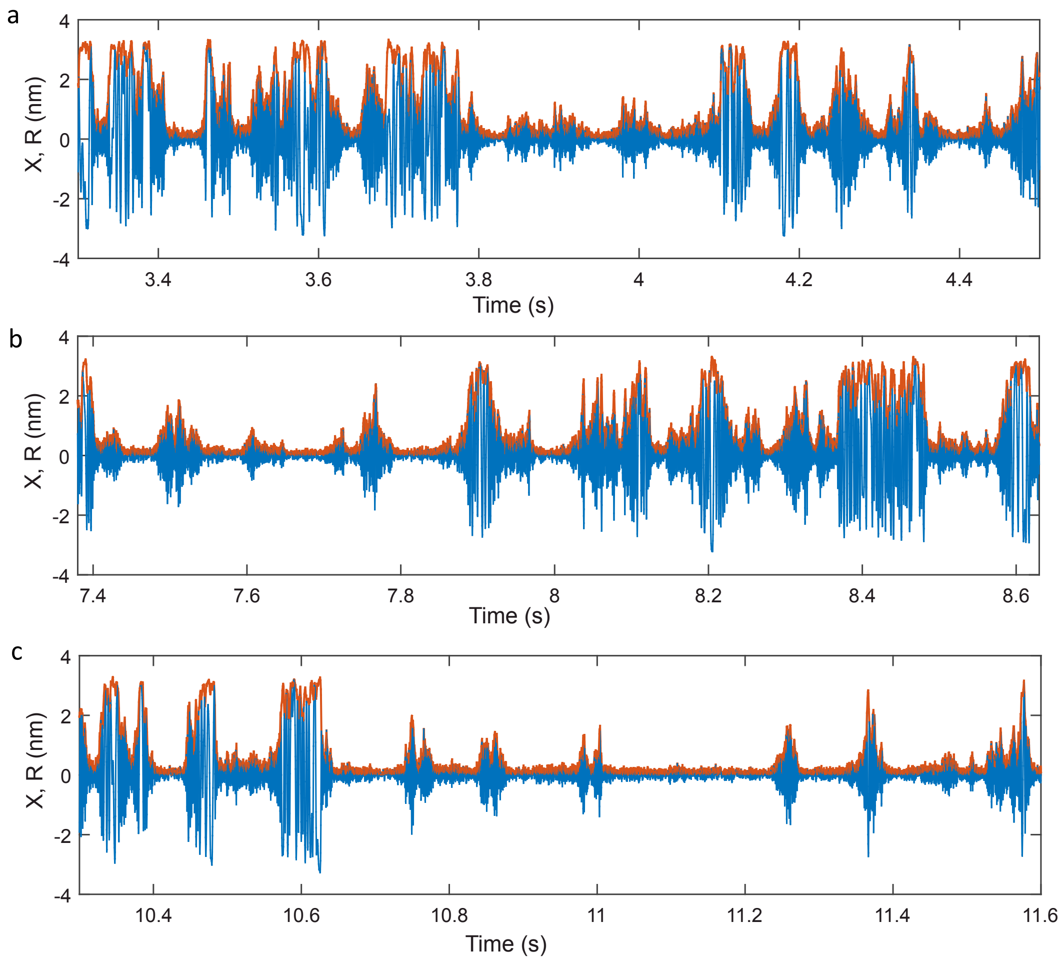

FIG. 4. **Time domain measurements. (a-c)** Three different time traces of one quadrature X (blue) and the corresponding amplitude R (orange) at $V_{\mathrm{sd}} = 0.25$mV for $V_{\mathrm{g}} = -616$mV, plotted from the Fig. 3h in the main text.

the total circuit and of the HEMT noise. This background contribution is independent of the source-drain voltage V_{sd}, so that it can be quantified from the current noise measured at $V_{\mathrm{sd}} = 0$ mV. After the substraction of this background contribution, we determine the Fano factor F of the nanotube device at finite V_{sd} from the measured current noise using $F = S_{\mathrm{II}}(V_{\mathrm{sd}})/(2eI_{\mathrm{sd}})$, where e is the electron charge, and I_{sd} is the DC current at a given source-drain bias V_{ds} (Fig. S6).

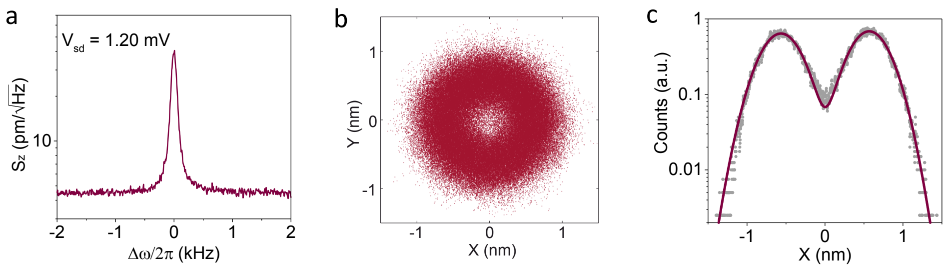

FIG. 5. **Pure self-oscillation.** **(a)** Displacement spectral density at $V_{\mathrm{sd}} = 1.2$ mV and $V_{\mathrm{g}} = -616$ mV. **(b)** The phase-space of the two quadratures of the motion. **(c)** Histogram associated to the phase-space in **b**.

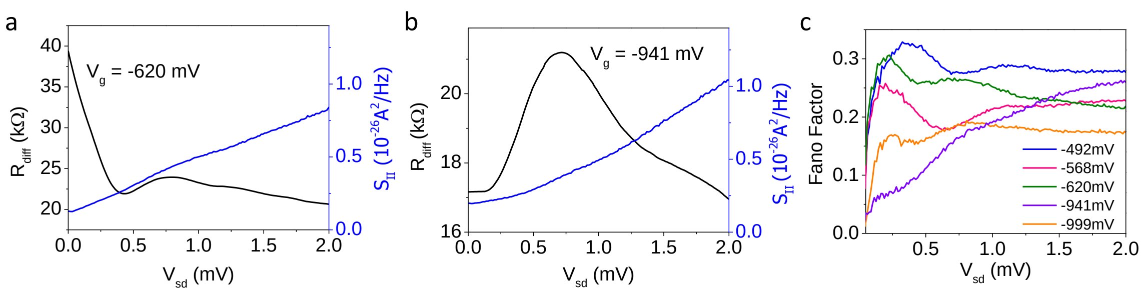

FIG. 6. **Shot noise measurements.** **(a,b)** Differential resistance R_{diff} (grey) and current noise density S_{II} (blue) as a function of V_{sd} for two different gate voltage values. **(c)** Fano factor as a function of V_{sd} for different V_{g} values.

V. DISPLACEMENT SENSITIVITY

The current noise floor $S_{\mathrm{I}}^{\mathrm{imp}}$ at ω_{RLC} sets the displacement imprecision noise $S_{\mathrm{z}}^{\mathrm{imp}}$ of the detection method using

$$S_{\mathrm{z}}^{\mathrm{imp}} = \left(\frac{1}{2} \frac{dG_{\mathrm{diff}}}{dV_{\mathrm{g}}} V_{\mathrm{g}} V_{\mathrm{sd}}^{\mathrm{ac}} \frac{C_{\mathrm{g}}'}{C_{\mathrm{g}}} \right)^{-1} S_{\mathrm{I}}^{\mathrm{imp}}. \tag{1}$$

The current noise floor at zero source-drain bias is given by the HEMT noise and the Johnson-Nyquist noise of the circuit. When increasing the bias, the contribution of the electron shot noise dominates the displacement sensitivity (Fig. S7a). The V_{sd} dependence of the imprecision displacement noise is obtained using Eq. 1 (Fig. S7b). The imprecision noise can reach the level of the displacement noise $S_{\mathrm{z}}^{\mathrm{zpf}} = \sqrt{2\hbar/m\omega_0\Gamma_{\mathrm{width}}}$ of the zero-point fluctuations at resonance frequency (Fig. S7c).

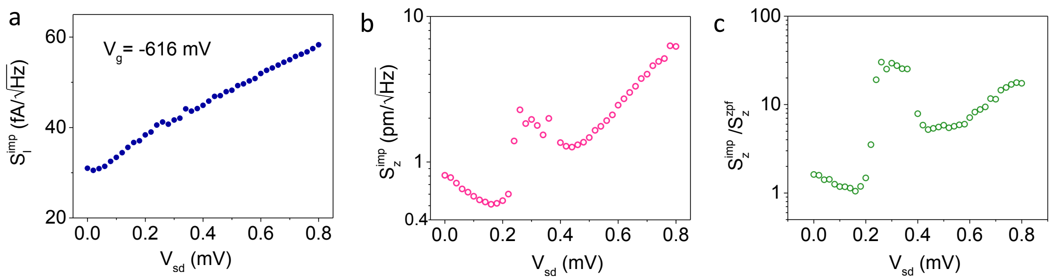

FIG. 7. **Displacement sensitivity. (a,b)** Current noise floor and displacement imprecision noise as a function of $V_{\rm sd}$. **(c)** Same as (b) but with the displacement imprecision noise normalised by the displacement noise of the zero-point fluctuations at resonance frequency.

VI. BACKACTION

A. Retardation time due to the circuit

Figure S8 shows the simplified electrical circuit used to evaluate the electrostatic and the electrothermal backactions when the retardation is given by the circuit. We consider the impedances relevant at the resonance frequency of the resonator. The nanotube with conductance G is connected on the source electrode to the capacitance $C_{\rm RC} \simeq 60$ pF of the coaxial cable and the resistance $R_{50} = 50\ \Omega$ of an attenuator, which form the impedance of the circuit

$$Z_{\rm T} = \left(R_{50}^{-1} + i\omega C_{\rm RC}\right)^{-1}. \tag{2}$$

The mechanical vibrations modulate the nanotube conductance by the amount δG. When a DC voltage $V_{\rm sd}$ is applied to the source electrode nanotube, the conductance modulation generates an oscillating current $\delta i_{\rm ac}$ at the frequency close to ω_0. The current flowing through $Z_{\rm T}$ creates an oscillating voltage $\delta v_{\rm ac}$ on the source electrode, so that

$$\delta v_{\rm ac} = -\delta i_{\rm ac} Z_{\rm T}, \tag{3}$$

$$\delta i_{\rm ac} = \delta G V_{\rm sd} + G\delta v_{\rm ac}. \tag{4}$$

Reference[1] made a similar analysis as here. The difference in the two analysis comes from the fact that our device is biased with a constant voltage, while the device in Ref.[1] is biased with a constant current.

The retardation time $\tau_{\rm RC}$ of the backaction on the vibrations is of the order of $1/\omega_0$. The retardation time is related to the delay of the modulation of $\delta v_{\rm ac}$ with respect to δG. We

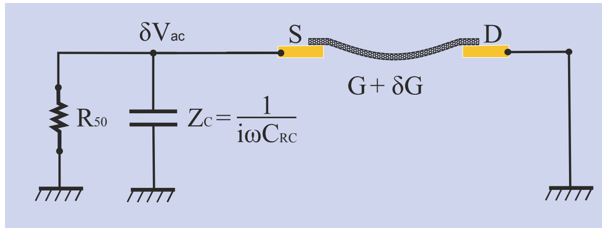

FIG. 8. **Simplified electrical circuit.**

thus express $\delta v_{\rm ac}$ as

$$\delta v_{\rm ac} = -\frac{Z_{\rm T}}{1+Z_{\rm T}G}\delta G V_{\rm sd} \simeq -R_{50}\frac{1-i\omega R_{50}C_{\rm RC}}{1+\omega^2 R_{50}^2 C_{\rm RC}^2}\delta G V_{\rm sd}, \tag{5}$$

where we use $R_{50}G << 1$ in the last equality. The argument of the complex number in the numerator is $\varphi = -\arctan\left(\omega R_{50}C_{\rm RC}\right)$, so that the retardation time is

$$\tau_{\rm RC} = \frac{\arctan\left(\omega_0 R_{50}C_{\rm RC}\right)}{\omega_0}. \tag{6}$$

From the values of $C_{\rm RC}$, R_{50}, and $\omega_0 \simeq 2\pi \cdot 92$ MHz, we get that $\omega_0 R_{50} C_{\rm RC} = 1.7$. Therefore, the retardation time $\tau_{\rm RC}$ of the circuit is of the order of $1/\omega_0$. The estimation $\omega_0\tau_{\rm RC} \sim 1$ is relevant, since this enhances cooling[2].

B. Electrostatic backaction with the retardation due to the circuit

As described in the last subsection, the modulation of the voltage $\delta v_{\rm ac}$ on the source electrode is due to the vibration-induced modulation of the conductance, when the nanotube is biased with a constant voltage. Assuming symmetric electrical contacts, the voltage modulation on the nanotube is $\delta v_{\rm NT} = \frac{1}{2}\delta v_{\rm ac}$. This results in the electrostatic force

$$\delta F = C_{\rm g}' V_{\rm g}\delta v_{\rm NT} = -\frac{1}{2}C_{\rm g}' V_{\rm g} R_{50}\frac{1-i\omega R_{50}C_{\rm RC}}{1+\omega^2 R_{50}^2 C_{\rm RC}^2}\frac{\partial G}{\partial z}V_{\rm sd}\delta z. \tag{7}$$

The real part of this backaction force leads to the shift of the spring constant, and the imaginary part to the shift of the decay rate. Using $F = -m\Delta\Gamma_{\rm back}\frac{dz}{dt}$ and $\frac{dz}{dt} = i\omega z$, we get

$$\Delta k_{\rm back} = \frac{1}{2}\left(\frac{R_{50}}{1+(R_{50}\omega C_{\rm RC})^2}\right)\frac{dG_{\rm diff}}{dV_{\rm g}}\frac{(C_{\rm g}'V_{\rm g})^2}{C_{\rm g}}V_{\rm sd}, \tag{8}$$

$$\Delta\Gamma_{\rm back} = -\frac{1}{2m}\left(\frac{R_{50}^2 C_{\rm RC}}{1+(R_{50}\omega C_{\rm RC})^2}\right)\frac{dG_{\rm diff}}{dV_{\rm g}}\frac{(C_{\rm g}'V_{\rm g})^2}{C_{\rm g}}V_{\rm sd}. \tag{9}$$

The retardation time of the backaction on the vibrations is about $1/\omega_0$.

This backaction cannot account for our data. Equation 9 cannot account for the efficient cooling in Figs. 4a,c of the main text, since the predicted $\Delta\Gamma$ is one order of magnitude smaller than that measured in Fig. 4d of the main text.

C. Electrothermal backaction with the retardation due to the circuit

The closed loop of the backaction goes as follows. The dissipated power increases the temperature of the device. The effective thermal expansion of the device leads to the displacement of the nanotube. This displacement reacts back on the dissipated power via $\delta G = \frac{\partial G}{\partial z}\delta z$. The delay of the retardation time is τ_{RC}.

The dissipated power of the voltage-biased nanotube is $P = (G + \delta G)(V_{\mathrm{sd}} + \delta v_{\mathrm{ac}})^2$. The first-order expansion of the power reads

$$\delta P_1 = V_{\mathrm{sd}}^2 \delta G - 2\frac{Z_{\mathrm{T}} G}{1 + Z_{\mathrm{T}} G} V_{\mathrm{sd}}^2 \delta G. \tag{10}$$

The first term of this equation leads to backaction when taking into account the thermalisation time of the device, as discussed in the next subsection. The second term results in the change of the decay rate because of the retardation of the circuit. This is what is discussed here.

The modulation of the dissipated power leads to the modulation of the mechanical tension in the nanotube. The tension modulation depends on the temperature profile along the nanotube and the electrodes, which is something hard to know precisely especially at low temperature when the electron transport is quasi-coherent[3]. In what follows, we assume for simplicity that the dissipation occurs solely in the nanotube, and that temperature rises by $\delta T = \delta P \tau_{\mathrm{ph}}/C_{\mathrm{heat}}$. Here, C_{heat} is the heat capacity of the nanotube and τ_{ph} is the thermalisation time of the nanotube. We do an additional simplification using $\tau_{\mathrm{ph}} \simeq L/v \simeq 0.1$ ns, where L is the nanotube length and $v \simeq 10^4$ m/s is the phonon velocity in nanotubes[4]. Assuming that the thermal expansion is solely occurring in the nanotube, the nanotube expands by $\frac{\delta L}{L} = \alpha_{\mathrm{TEC}}\delta T$ where α_{TEC} is the thermal expansion coefficient of the nanotube. Using Hook′s law, the change of the mechanical tension is given by $\delta T_{\mathrm{mech}} = 2\pi r E_{\mathrm{2d}} \frac{\delta L}{L}$ where $E_{\mathrm{2d}} = 340$ N/m is the two-dimensional Young′s modulus of graphene and r the nanotube radius. Overall, the mechanical tension is related to the dissipated power by

$$\delta T_{\mathrm{mech}} = \frac{\alpha_{\mathrm{TEC}} E_{\mathrm{2d}} \tau_{\mathrm{ph}}}{C_{\mathrm{heat}}} 2\pi r \delta P_1. \tag{11}$$

We emphasize that we would get a linear relation between the tension and the power as in Eq. 11 albeit with a different ratio $\delta T_{\mathrm{mech}}/\delta P_1$, if we were considering dissipation in the electrodes and/or thermal expansion of the electrodes.

The modulation of the mechanical tension generates a shift in the spring constant and in the decay rate. For this, we use the Euler-Bernoulli equation that reads

$$\rho S\frac{d^2Z}{dt^2} = -EI\frac{d^4Z}{dx^4} + \left[T_{\mathrm{mech}} + \frac{ES}{2L}\int_0^L \left(\frac{dZ}{dx}\right)^2 dx\right]\frac{d^2Z}{dx^2} \tag{12}$$

where ρ is the nanotube mass density, S the nanotube cross-sectional area, Z the displacement at the coordinate x along the nanotube axis, t the time, E the nanotube three-dimensional Young′s modulus, and I the moment of inertia. We assume that the restoring force is solely given by the mechanical tension, as it is the case in our experiment, so that $EI\frac{d^4Z}{dx^4} \to 0$. We set

$$Z(x,t) = z_{\mathrm{s}} \times \phi_{\mathrm{s}}(x) + z_1(t) \times \phi_1(x). \tag{13}$$

Here, $\phi_{\mathrm{s}}(x)$ and $\phi_1(x)$ are the profiles of the static deformation and the measured eigenmode with $\max(\phi_{\mathrm{s}}(x)) = \max(\phi_1(x))$=1, whereas z_{s} and $z_1(t)$ are the associated time dependent displacements. We use $\phi_{\mathrm{s}}(x) = \phi_1(x) = \sin(\pi x/L)$, a good approximation since the nanotube is under tensile tension. The equation of motion is obtained by multiplying the Euler-Bernoulli equation by $\phi_1(x)$ and integrating it along x. The mechanical tension is $T_{\mathrm{mech}} = T^0_{\mathrm{mech}} - \delta T_{\mathrm{mech}}$ where T^0_{mech} is the time-independent tension in the nanotube. The time-dependent tension creates a term proportional to z_1. The real part of this term induces a shift in the spring constant, and the imaginary part leads to a shift in the decay rate,

$$\Delta k_{\mathrm{back}} = \alpha m\frac{1}{C_{\mathrm{RC}}R_{50}}\frac{dG_{\mathrm{diff}}}{dV_{\mathrm{g}}}\frac{C'_{\mathrm{g}}}{C_{\mathrm{g}}}V_{\mathrm{g}}z_s V_{\mathrm{sd}}^2, \tag{14}$$

$$\Delta\Gamma_{\mathrm{back}} = -\alpha\frac{dG_{\mathrm{diff}}}{dV_{\mathrm{g}}}\frac{C'_{\mathrm{g}}}{C_{\mathrm{g}}}V_{\mathrm{g}}z_s V_{\mathrm{sd}}^2, \tag{15}$$

$$\alpha = \frac{\pi^3 r}{L}\frac{\alpha_{\mathrm{TEC}}E_{2\mathrm{d}}\tau_{\mathrm{ph}}}{C_{\mathrm{heat}}}\frac{1}{m}\left(\frac{2C_{\mathrm{RC}}GR_{50}^2}{(\omega C_{\mathrm{RC}}R_{50})^2+1}\right). \tag{16}$$

The retardation time of the backaction on the vibrations is about $1/\omega_0$, that is, $\tau \simeq 2$ ns.

We now compare the measurements of the decay rate as a function of V_{sd} in Fig. 3b and Fig. 4d with Eq. 15 (pink lines). We estimate that the static displacement is $z_s = -0.97$ nm at $V_{\mathrm{g}} = -616$ mV and $z_s = -2.08$ nm at $V_{\mathrm{g}} = -943$ mV using $z_s = -\frac{4}{\pi}\frac{C'_{\mathrm{g}}V_{\mathrm{g}}^2}{m\omega_0^2}$ from the derivation of the Euler-Bernoulli equation. We use $C_{\mathrm{heat}} = 1.6 \cdot 10^{-22}$ J/K from Ref.[5] where the specific heat capacity of nanotubes is $3 \cdot 10^{-5}$ J/gK at 0.1 K. The only free parameter left is the thermal expansion coefficient. From the comparison between the measurements and this model, we get $\alpha_{\mathrm{TEC}} = 9 \cdot 10^{-8}$ 1/K. Although we did not find any report on α_{TEC} for nanotubes, graphene, and graphite at such low temperatures, the order of magnitude that we get is rather realistic. The temperature modulation involved in the backaction at $V_{\mathrm{g}} = -943$ mV is estimated to be 40 μK and 0.4 mK at $V_{\mathrm{sd}} = 0.1$ mV and $V_{\mathrm{sd}} = 0.565$ mV, respectively.

To finish this subsection, we discuss the third-order expansion of the power modulation related to Eq. 10, since it is relevant for the self-oscillation regime. The third-order expansion reads

$$\delta P_3 = V_{\mathrm{sd}}^2 \delta G^3 \left(\frac{Z_{\mathrm{T}}}{1 + Z_{\mathrm{T}} G} \right)^2 . \tag{17}$$

Carrying out the same derivation as that described above, we obtain two additional backaction force terms, that is, a Duffing force and a nonlinear decay force of the form $z^2 \frac{dz}{dt}$. Depending on the sign of $\frac{dG_{\mathrm{diff}}}{dV_{\mathrm{g}}}$, the nonlinear decay force can be negative, so that this force further increases the amplification, especially when the amplitude of motion is large. The exact derivation of the nonlinear decay force is difficult due to its renormalisation by the other nonlinear forces. The study of this nonlinear force is beyond the scope of this Letter.

D. Electrothermal backaction with the retardation due to the thermalisation time of the device

In contrast to the backaction discussed in the last subsection, this backaction arises from the modulation of the power $\delta P_1 = V_{\mathrm{sd}}^2 \delta G$ in Eq. 10 associated to the thermalisation time of the device. The derivation of the backaction is similar to that above. The time-dependent tension that is induced by δP_1 creates a force F proportional to z_1 in the equation of motion. The shift in the decay rate is given by $\Delta\Gamma_{\mathrm{back}} = \frac{1}{m} \frac{\partial F}{\partial z_1} \tau_{\mathrm{ph}}$ when the thermalisation time τ_{ph} is much shorter than ${\omega_0}^2$. As a result, we obtain

$$\Delta\Gamma_{\mathrm{back}} = -\alpha \frac{dG_{\mathrm{diff}}}{dV_{\mathrm{g}}} \frac{C'_{\mathrm{g}}}{C_{\mathrm{g}}} V_{\mathrm{g}} z_s V_{\mathrm{sd}}^2, \tag{18}$$

$$\alpha = \pi^3 \frac{r}{Lm} \frac{\alpha_{\mathrm{TEC}} E_{\mathrm{2d}} \tau_{\mathrm{ph}}^2}{C_{\mathrm{heat}}}. \tag{19}$$

When we compare the measured V_{sd} dependence of the decay rate with this model, the agreement is satisfactory. The functional form of Eq. 18 is the same as that in Eq. 15 when the retardation is due to the circuit. From the comparison between the measurements and this model, we get $\alpha_{\mathrm{TEC}} = 3 \cdot 10^{-9}$ 1/K, which is smaller that the value obtained when the retardation is due to the circuit. The temperature modulation involved in the backaction at $V_{\mathrm{g}} = -943$ mV is estimated to be 0.8 mK and 9 mK at $V_{\mathrm{sd}} = 0.1$ mV and $V_{\mathrm{sd}} = 0.565$ mV, respectively.

[1] Steeneken, P. G. *et al.* Piezoresistive heat engine and refrigerator. *Nature Phys.* **7**, 354–359 (2011).

[2] Metzger, C. H. & Karrai, K. Cavity cooling of a microlever. *Nature* **432**, 1002–1005 (2004).

[3] Datta, S. *Electronic Transport in Mesoscopic Systems* (Cambridge University Press, 1996).

[4] De Martino, A., Egger, R. & Gogolin, A. O. Phonon-phonon interactions and phonon damping in carbon nanotubes. *Phys. Rev. B* **79**, 205408 (2009).

[5] Hone, J., Batlogg, B., Benes, Z., Johnson, A. T. & Fischer, J. E. Quantized phonon spectrum of single-wall carbon nanotubes. *Science* **289**, 1730–1733 (2000).